Mutual repression between proliferation and plant invasion is mediated by a master regulator of appressorium formation in the corn smut fungus *Ustilago maydis*.

SUPPLEMENTARY MATERIAL

Antonio de la Torre, Sónia Castanheira, and José Pérez-Martín*
Instituto de Biología Funcional y Genómica. Consejo Superior de Investigaciones Científicas. Salamanca. Spain

SI Materials and Methods

Plasmid Constructions

Serine or threonine to alanine mutant variants were constructed as replacement cassettes carrying the desired mutation (associated to the appearance or loss of a restriction enzyme target for diagnostic purposes) to be inserted by homologous recombination into the endogenous locus. The cassette also allowed the insertion of a resistance to hygromycin, flanked by FRT sites to remove the resistance cassette once the endogenous locus was mutated, following published procedures (1).

To replace native *hdp2* allele with the *hdp2*^{T607A} allele, we constructed a gene replacement cassette using Golden Gate assembly, following published procedures (2). The 5' fragment, carrying the desired mutation (2051 bp) was produced by PCR-based mutagenesis (four-primer PCR with internal mutagenic primers) and it was assembled from two fragments: the left fragment (627 bp) was amplified with the primer pair HDP2-1/HDP2-2 and the right fragment (1479 bp) was amplified with the primer pair HDP2-3/HDP2-4. The inserted mutation was a change in the codon number 691 (ACG to GCG), which was associated to the loss of the restriction site for *Rse*I. The 3' fragment (463 bp) was obtained by genomic PCR with the primer pair HDP2-5/HDP2-6.

To replace native *biz1* with the *biz1*$^{S663A\ T691A}$ alleles, we also constructed a gene replacement cassette using Golden Gate assembly. The 5' fragment consisted of a synthetic 922 bp DNA fragment that includes the two desired mutations: codon 663 (TCG to GCT) and codon 691 (ACG to GCG). The mutation in codon 663 resulted in the formation of a recognition site for *Afe*I. This DNA fragment was also flanked by *Bsa*I recognition sites compatible with

the vectors used in the Golden Gate assembly. The 3' fragment (899 bp) was obtained by genomic PCR with the primer pair BIZ1-1/BIZ1-2.

To construct single codon substitutions in Biz1, we exchanged, in the 922 bp synthetic DNA carrying the two mutations, fragments with the respective wild-type versions upon digestion with *Nco*I+*Sac*I (to exchange codon 663) or *Sac*I+*Cla*I (to exchange codon 691). The respective single mutant fragments were assembled using Golden Gate assembly as above.

To replace native *biz1* with the *biz1*$^{S663D\ T691D}$ allele, we also constructed a gene replacement cassette using Golden Gate assembly using a 5' fragment consisting of a synthetic 922 bp DNA fragment that includes the two desired mutations: codon 663 (TCG to GAC) and codon 691 (ACG to GAT). The mutation in codon 663 resulted in the formation of a recognition site for *Psu*I.

To construct the *biz1* allele under the control of P_{crg1} promoter (*biz1*^{crg1}), we also used a Golden Gate assembly as described. The 5' fragment (1062 bp) and 3' fragment (1114 pb) were obtained by genomic PCR with the primer pairs BIZ1CRG-1/BIZ1CRG-2 and BIZ1CRG-3/BIZ1CRG-4 respectively.

To construct the C-terminal fusion of Biz1 to GFP or 3HA we also used a Golden Gate assembly as described. The 5' fragment (1108 bp) and 3' fragment (899 bp) were obtained by genomic PCR with the primer pairs BIZ1GFP-1/BIZ1GFP-2 and BIZ1GFP-3/BIZ1GFP-4 respectively.

Strains used in each experiment.

Fig. 1. (B) FB1, FB2, UMS123, UMS125, UMP368, UMP369, UMP370, UMP371, UMP364, UMP367, UMP365, UMP366. (C) SG200AM1, UMP367, UMP365, UMP366. (D) UMP560.

Fig. 2. (B) FB1, UMC10, UMP382, UMP390, UMP386, UMP400. (C) AUM331, AUM333, AIUM332, AUM335. (D) UMP120, UMP433, UMP434, UMP437. (E) AB34, UMP112, UMS120, UMP431, UMP432, UMP433, UMP434, UMP436, UMP437.

Fig. 3. (A) UMP382, UMP383, UMP384. (C) UMP382, UMP386, UMP390, UMP400, UMP384, UMP397, UMP392, UMP393.

Fig. 4. (A) AUM346, AUM349, AUM347, AUM348. (B) AUM349, UMP568. (C) UMP406, UMP407, UMP408, UMP409.

Fig. 5. (B) UMP363, UMP520. (C) UMP363, UMP520. (D) SG200, UMS131, UMS360, UMN69, UMP500, UMP501, UMP502, UMP503.

Fig. S1. SG200AM1, UMS154, UMS155, UMS156, UMS186, UMS187.

Fig. S2. SG200, UMS131, UMP500, UMP565, UMP566, UMP567.

Fig. S3. UMP363, UMS191, UMS154, UMP571.

Fig. S4. SG200, UMS131, UMP500.

Fig. S5. FB1, FB2, UMS364, UMS367, UMS123, UMS125, UMP365, UMP366.

Fig. S6. SG200AM1, UMS154, UMP361, UMP363.

Fig. S7. UMP112, UMP431, UMS120, UMP433.

Fig. S8. AB34, AB33, UMP431, UMS120, UMP433.

Fig. S9. AUM331, AUM332, AUM333, AUM335.

Fig. S10. UMP112, UMS120, UMP431, UMP432, UMP433, UMP434, UMP436, UMP437.

Fig. S11. AUM346, AUM347, AUM348, AUM349.

Fig. S12. UMP520.

FIGURE S1

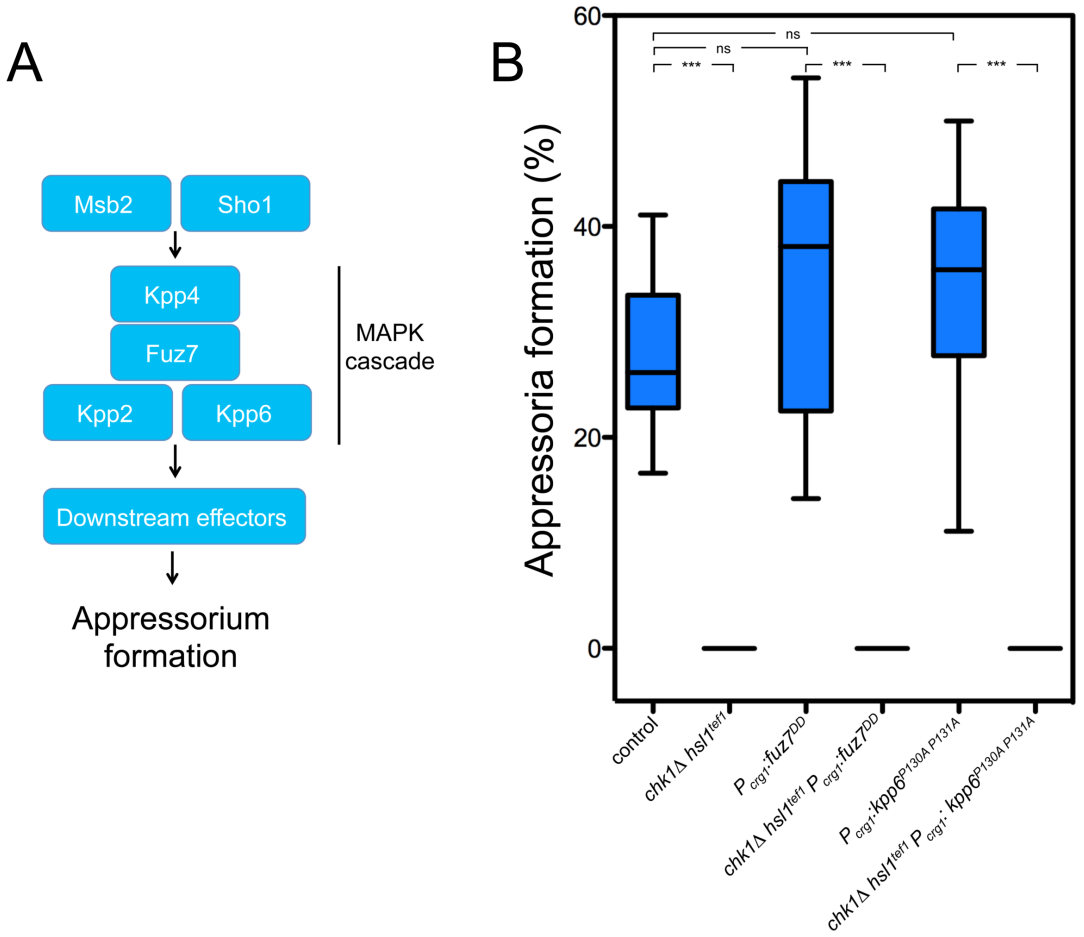

Fig. S1. Cell cycle regulation seems to interfere with elements downstream the signaling cascade responsible to activate the formation of appressoria.

A. Scheme of the genetic pathway responsible of appressorium formation in *U. maydis*. The activation of the program that produces differentiation of the infective filament into the appressorium involves the sensing of plant-derived stimuli by two membrane proteins, Sho1 and Msb2 (3), which transmit the signal by a well-characterized MAPK cascade (4). Mutants lacking these elements are severely impaired in their capacity to produce appressoria and subsequently showed dramatic defects in virulence. Downstream of this signaling cascade, a plethora of transcription factors seems to be required to

activate the transcriptional program responsible for the appressorium formation (5).

B. Gain-of-function mutants in the MAPK cascade do not bypassed the cell cycle arrest requirement during *in vitro* appressorium formation. Incubation of solopathogenic strains (i. e. independent of the mating step, derived from SG200 strain, (6)) on hydrophobic surfaces in the presence of 16-hydroxyhexadecanoic acid (the cutin monomer), resulted in the induction of appressorium formation (4). Because the appressorium from *U. maydis* is a simple slight swelling of the infective filament, not easy to distinguish by morphological criteria, to facilitate the localization of appressoria, these solopathogenic strains carried a fluorescent reporter of appressorium formation (AM1-GFP). The AM1-GFP reporter is a transcriptional GFP fusion with the promoter from the gene encoding um0779. This marker shows GFP expression exclusively in those tip cell of filaments that differentiate an appressorium (4).

To address at which level (upstream or downstream of the signaling cascade) an active cell cycle interferes with the appressorium formation, we have analyzed whether the bypass of the MAPK signaling was able to disable the inhibition of appressorium formation by an active cell cycle. For that, we inserted two distinct constructions aimed to activate the MAPK cascade at different levels into a solopathogenic strain carrying the two mutations disabling the b-dependent cell cycle arrest (*chk1*Δ and *hsl1*^{tef1}). As control, we introduce the same constructions into a wild-type strain. These constructions expressed, under the control of the *crg1* promoter (induced by the presence of arabinose), either the *fuz7*^{DD} allele, encoding a version of the pheromone cascade MAPK kinase, which is independent of upstream activation (7) or the *kpp6*$^{P130A\ P131A}$ allele, which is a MAPK version partially independent of the requirement of membrane sensor Sho1(3). We have spread the respective strains carrying the AM1-GFP reporter on an artificial hydrophobic surface (Parafilm) in the presence of long-chain hydroxy fatty acids and arabinose. After 20 hours of incubation, we have scored the proportion of filaments (stained with CFW) showing GFP fluorescence (i. e. adopting the appressorium differentiation program). The graph shows the result from three independent experiments, counting more than 50 filaments each. We have observed that no one of the tested mutants showed a suppression of the repressive effect of an active cell

cycle into the appressorium formation *in vitro*. These results suggested that the inhibitory signal emanating from an active cell cycle most likely was not affecting the signaling cascade and that, probably, the putative targets of the cell cycle regulation were located downstream of the MAPK cascade.

FIGURE S2

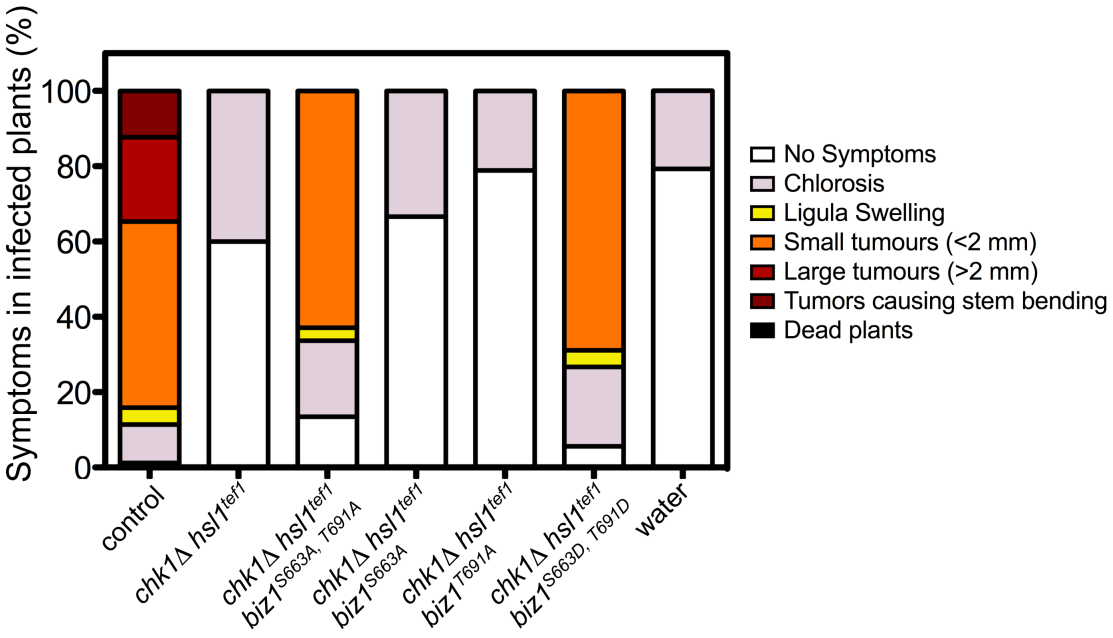

Fig. S2. The suppression of the lack of virulence in *hsl1^{tef1} chk1*Δ mutants required the two Ser/Thr to Ala substitutions in Biz1.

Graph showing disease symptoms caused by the indicated solopathogenic strains (SG200-derived) carrying different *biz1* alleles. The symptoms were scored 14 days after infection. Three independent experiments were carried out and the average values are expressed as percentage of the total number of infected plants (n: 30 plants in each experiment, see Table S4 for raw data). While the double Ser/Thr to Ala substitution (*biz1$^{S663A,\ T691A}$*) was able to suppress the lack of virulence of *chk1*Δ and *hsl1^{tef1}* mutants, the single substitutions (*biz1^{S663A}* or *biz1^{T691A}*) failed to do so. Phosphomimetic substitutions (Ser/Thr to Asp, *biz1$^{S663D,\ T691D}$*) behaves as the double phosphodead mutant. These results are coherent with the interaction, described in this work, with 14-3-3 protein once Biz1 is phosphorylated. 14-3-3 proteins

showed higher affinity to dual binding sites in their targets, although they are still able to bind to single sites (8), and it has been reported that glutamate and aspartate do not provide good phosphomimetic residues with respect to 14-3-3 binding to target proteins and resulted in phosphodead mutations (9).

FIGURE S3

A

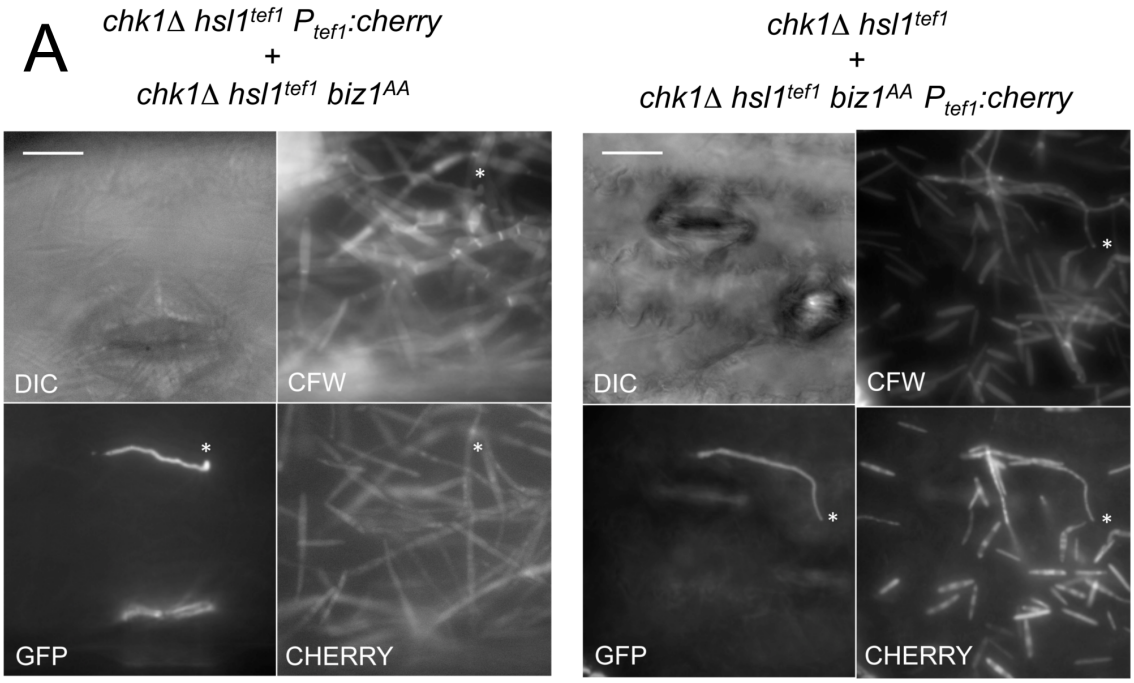

B

Infection mixture	GFP + filaments	Cherry + filaments
chk1Δ hsl1^{tef1} P_{tef1}*:cherry* + *chk1Δ hsl1*^{tef1} *biz1*^{AA}	37	0
chk1Δ hsl1^{tef1} + *chk1Δ hsl1*^{tef1} *biz1*^{AA} P_{tef1}*:cherry*	24	24

Fig. S3. *chk1Δ hsl1*^{tef1} mutants carrying the *biz1*^{AA} allele were able to produce appressoria on plant.

To address whether the presence of Biz1^{AA} was able to recover the ability of *chk1Δ hsl1*^{tef1} mutants to produce appressoria on plant, we used the strategy

depicted in (10), which allows the direct comparison of two different strains in the same conditions. Basically, we co-infected plants with equal numbers of two distinct SG200-derived cells carrying the appressorium reporter AM1-GFP. In one experiment class (left panel), the double *chk1*Δ *hsl1*^{tef1} strain carrying in addition a transgene that constitutively expressed a cherry fluorescent marker was mixed with the triple *chk1*Δ *hsl1*^{tef1} *biz1*^{AA} mutant. In the second experiment class (right panel), we reversed the mixture of strains, being the triple mutant strain the one that carried the cherry marker. After 1 dpi, fungal material on the leaf surface was stained with calcofluor white (CFW) and expression of AM1 (GFP fluorescence) was scored with respect to specific cherry fluorescence.

A. Panels showing the indicated strain combinations. The asterisk marks the presence of appressorium on the plant surface. Bar: 30 μm.

B. Quantification of the total number (from two independent experiments) of detected appressoria (filaments with GFP signal), indicating the number of them showing cherry fluorescence in the two different strain combinations. Note that appressorium formation was always associated to the triple mutant and never was observed with the double mutant.

FIGURE S4

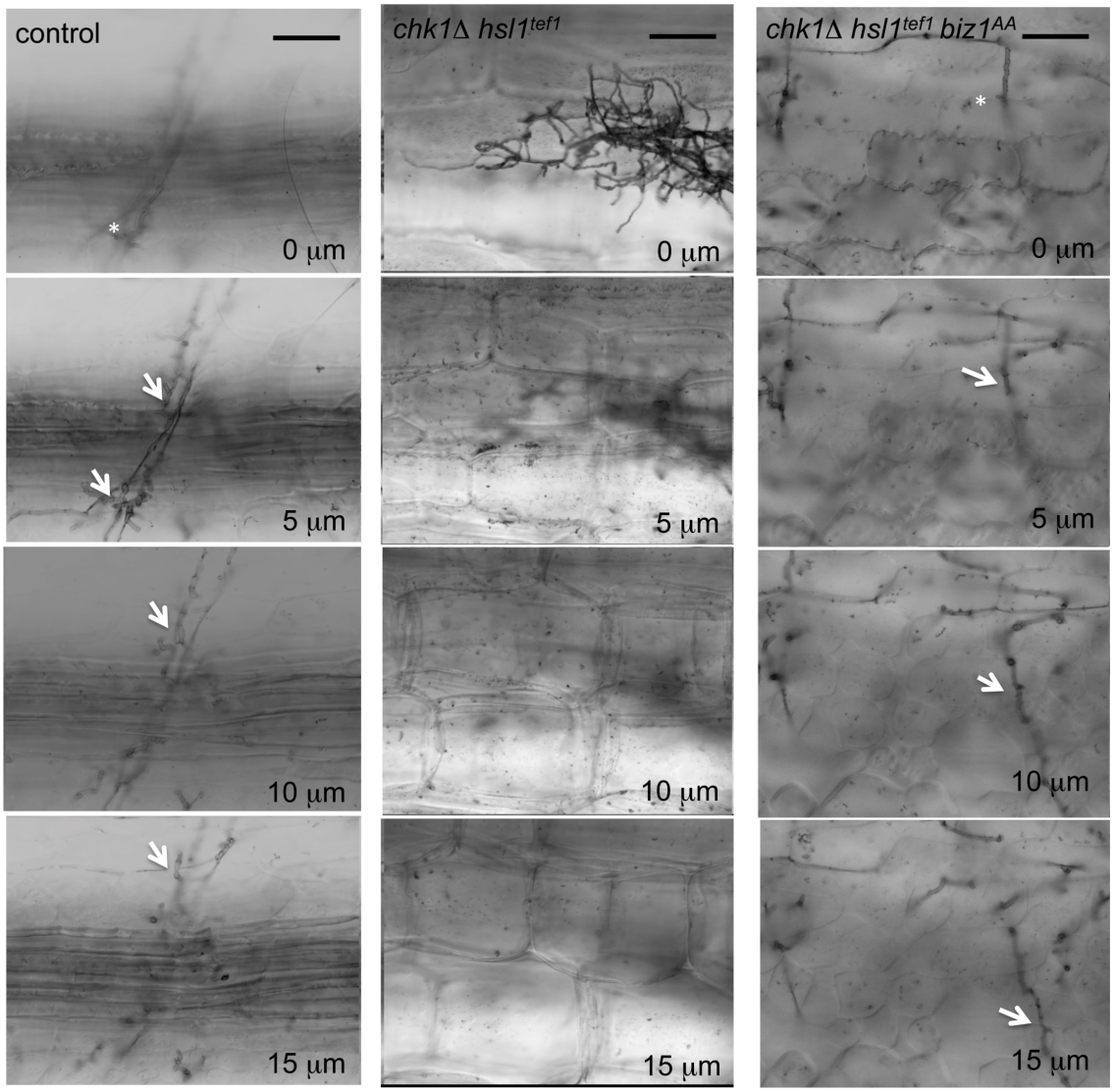

Fig. S4. *chk1*Δ *hsl1*^{tef1} mutants carrying the *biz1*^{AA} allele were able to penetrate the plant tissue.

Series of z axis projections showing the infection of wild-type (SG200) (left pannel), double mutant (middle panel), and triple mutant (right panel) solopathogenic strains. Corn leaves showing symptoms (chlorotic areas in the case of double mutant) were collected at day 5 after infection and fungal material was visualized by staining with Chlorazole Black (11). We followed through the z axis the presence of fungal material inside the plant tissue

(arrows). The point of penetration is marked by an asterisk. Note that the double mutant was unable to penetrate and it seem to proliferate on the surface of the plant. Bar: 25 μm.

FIGURE S5

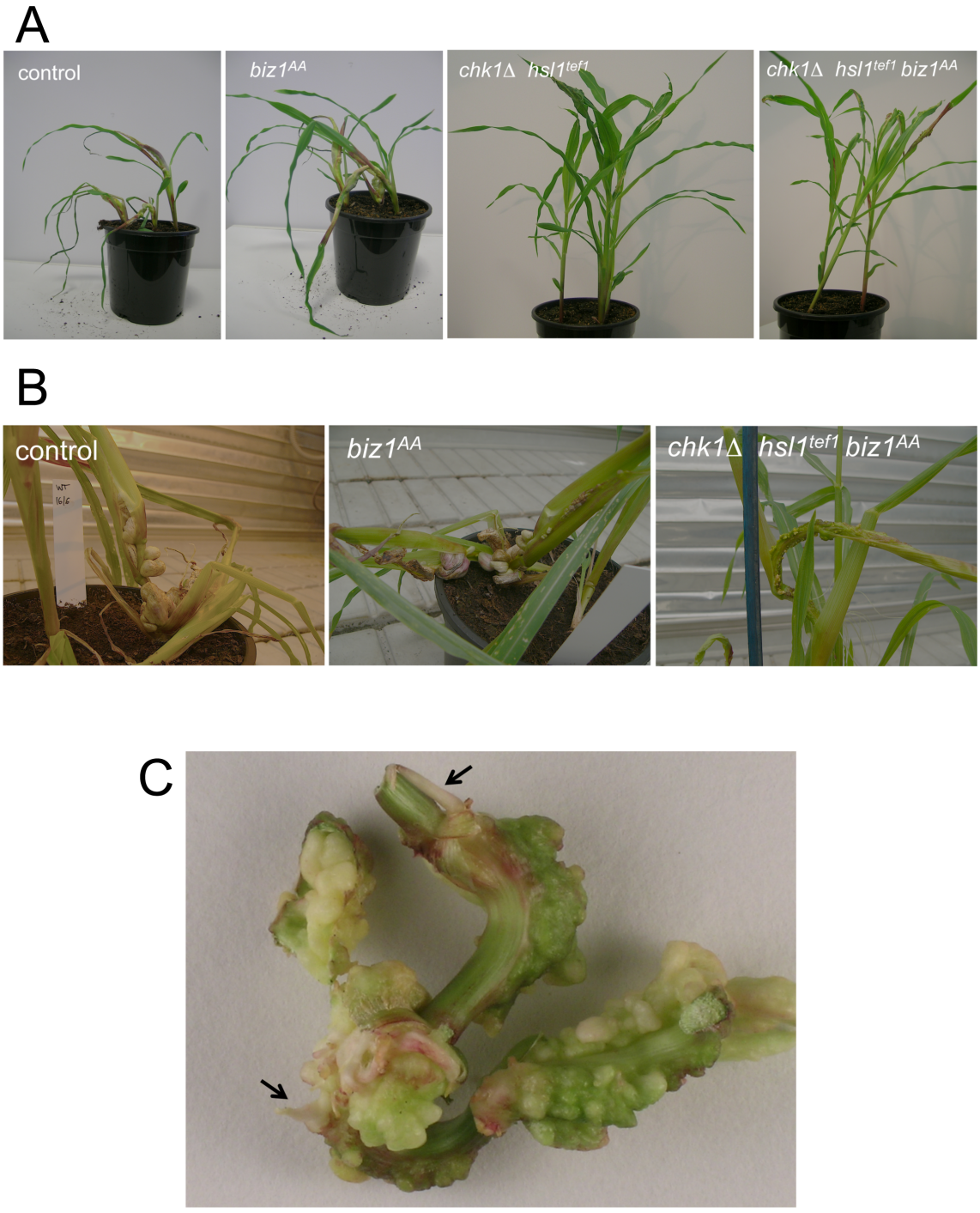

Fig. S5. Macroscopic symptoms of plants infected with strains carrying Biz1^{AA}.

A. Representative images of plants infected with the corresponding crosses. Plants were photographed 8 dpi.

B. Morphology of tumours caused by crosses of wild-type (control), *biz1^{AA}* and triple *chk1*Δ *hsl1^{tef1} biz1^{AA}* mutant. Tumours were photographed at 16 dpi.

C. Image showing tumours produced by the infection with the triple *chk1*Δ *hsl1^{tef1} biz1^{AA}* mutant. Note the presence of small, shoot-like structures (arrows) in some tumors.

Plants infected with the triple mutant cross do not showed big tumors. We believe that the less severe symptoms observed by the triple mutant infections were attributable to the lack of Chk1 activity, more than some possible effect of Biz1^{AA}. We base this assumption in two observations: in first place, plants infected with strains carrying the *biz1^{AA}* allele alone presented tumors that were similar to those observed from wild-type infections. Secondly, a striking feature observed in tumors induced by *chk1*Δ *hsl1^{tef1} biz1^{AA}* strains is the development of small, shoot-like structures (arrows). Such structures were described previously in plants infected by *U. maydis* mutants lacking either Chk1 or Atr1 kinases, which were required for the correct fungal development inside the plant (12), basically because they control the cell cycle during dikaryotic growth of basidiomycetes (13).

FIGURE S6

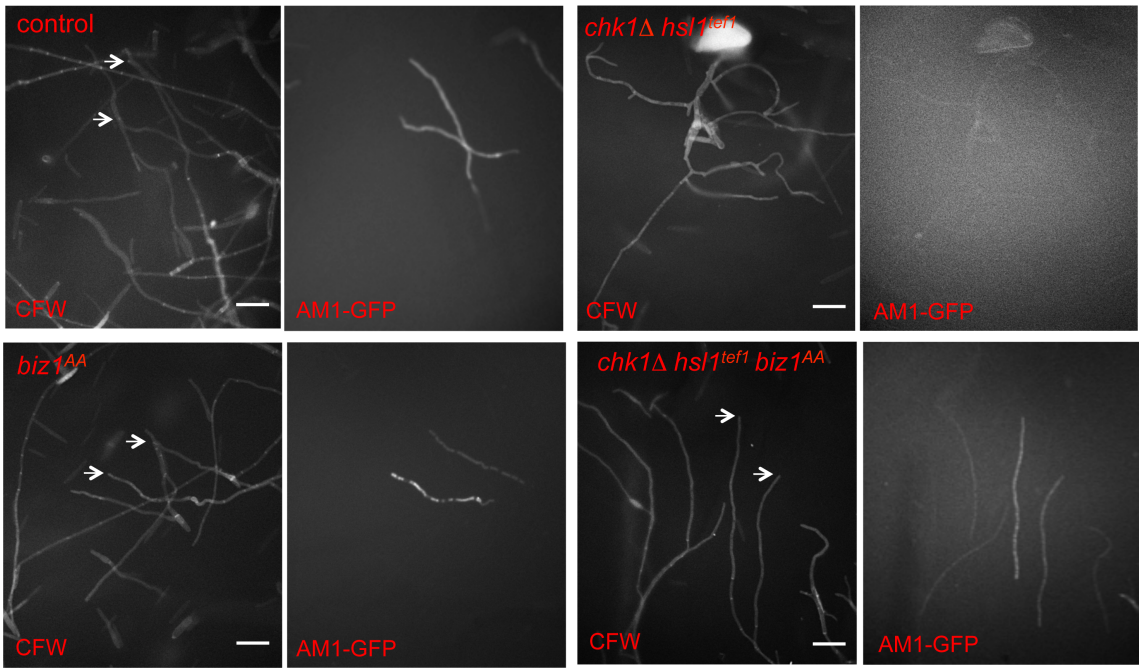

Fig. S6. Appressoria formation in vitro.

Micrographs to show *in vitro* appressoria formation from control strain as well as from the strain carrying the *biz1*^{AA} allele and the mutations disabling the cell cycle arrest. All the strains carried the appressorium-specific AM1-GFP reporter. Cells were stained with Calcofluor White (CFW) and analyzed for AM1 marker expression (AM1-GFP). The arrows pointed the tip of filaments forming appressorium. Scale bar, 20 μm.

FIGURE S7

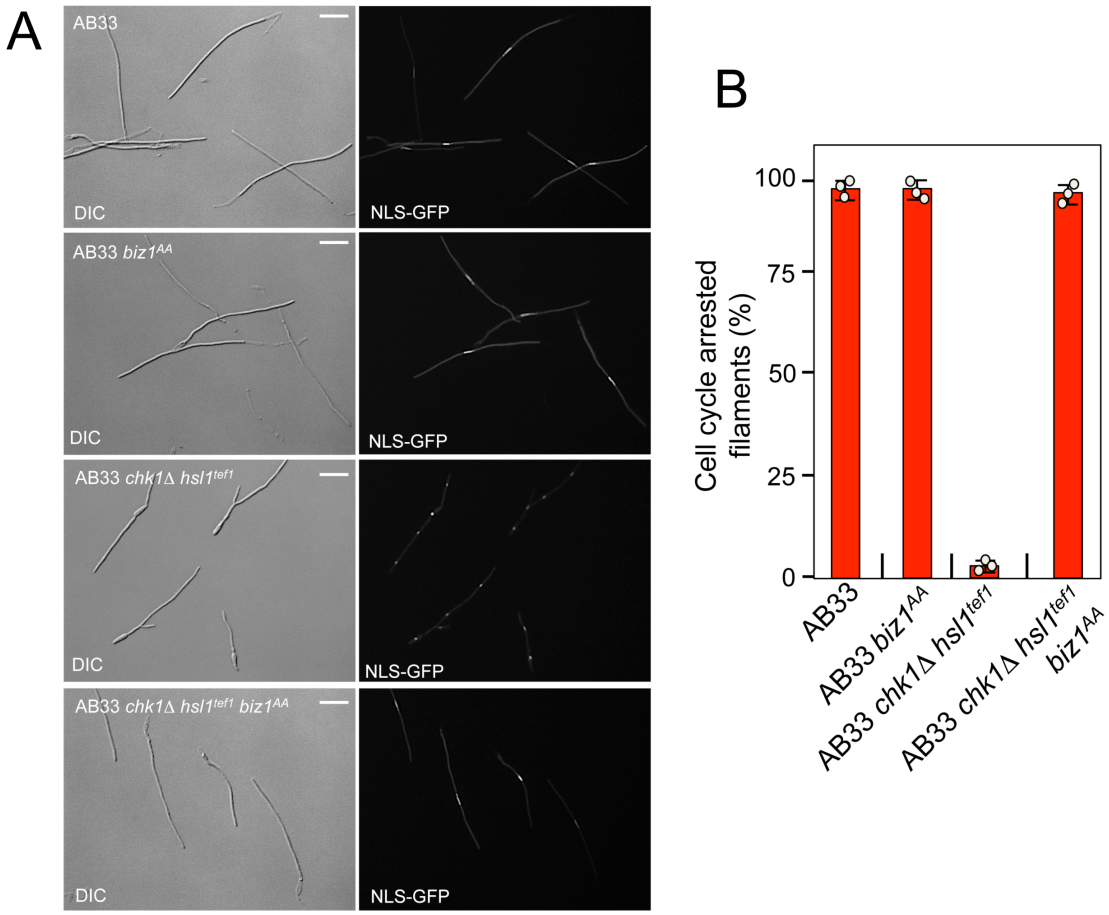

Fig. S7. The presence of Biz1^{AA} arrest the cell cycle in the infective filaments that disconnect the b- program from cell cycle regulation.

AB33-based strains carrying the indicated mutations were incubated for 8 hours in minimal medium amended with nitrate to induce the genes encoding the b-factor (which are under the control of the *nar1* promoter (14)). These strains also carried an NLS-GFP transgene as a nuclear marker to address the nuclear number of each filament. Filaments carrying a single nucleus were considered as arrested on cell cycle (15). (A) Representative images of cultures from the indicated strains. Bar: 20 μm. Note that the triple mutant cells were cell cycle arrested at the same extent as the control strain (AB33) in similar conditions.

(B) Graph shows the quantification of the nuclear content of filaments. Data are presented as mean ± SD from three independent experimental replicates counting more than 50 filaments each.

FIGURE S8

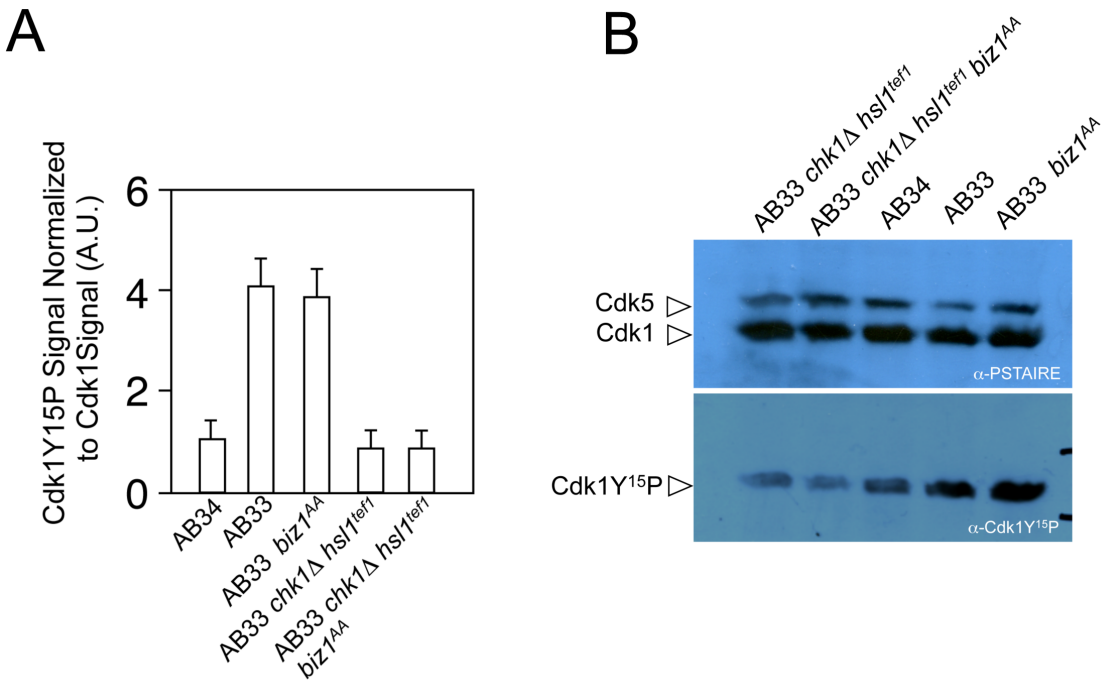

Fig. S8. Biz1^{AA} does not alter the level of Cdk1 inhibitory phosphorylation. AB33-derived cells carrying the indicated mutations were grown for 8 hours in inducing conditions for b-factor (nitrate minimal medium) and samples were taken and submitted to Western blot analysis. Immunoblots were incubated successively with an antibody that recognizes the Cdk1 phosphorylated form (anti-Cdk1-Y^{15}P) and anti-PSTAIRE, which recognizes both Cdk1 and Cdk5. Levels of Cdk1 phosphorylation were determined by quantifying the level of antibody signal using a ChemiDoc (Bio- Rad). Differences in loading of samples were corrected by dividing each phosphopeptide-specific antibody signal by the Cdk1 (anti-PSTAIRE) antibody signal. This experiment was carried out three independent times and the values shown in panel A are the average from these repeats. Panel B showed a representative gel.

FIGURE S9

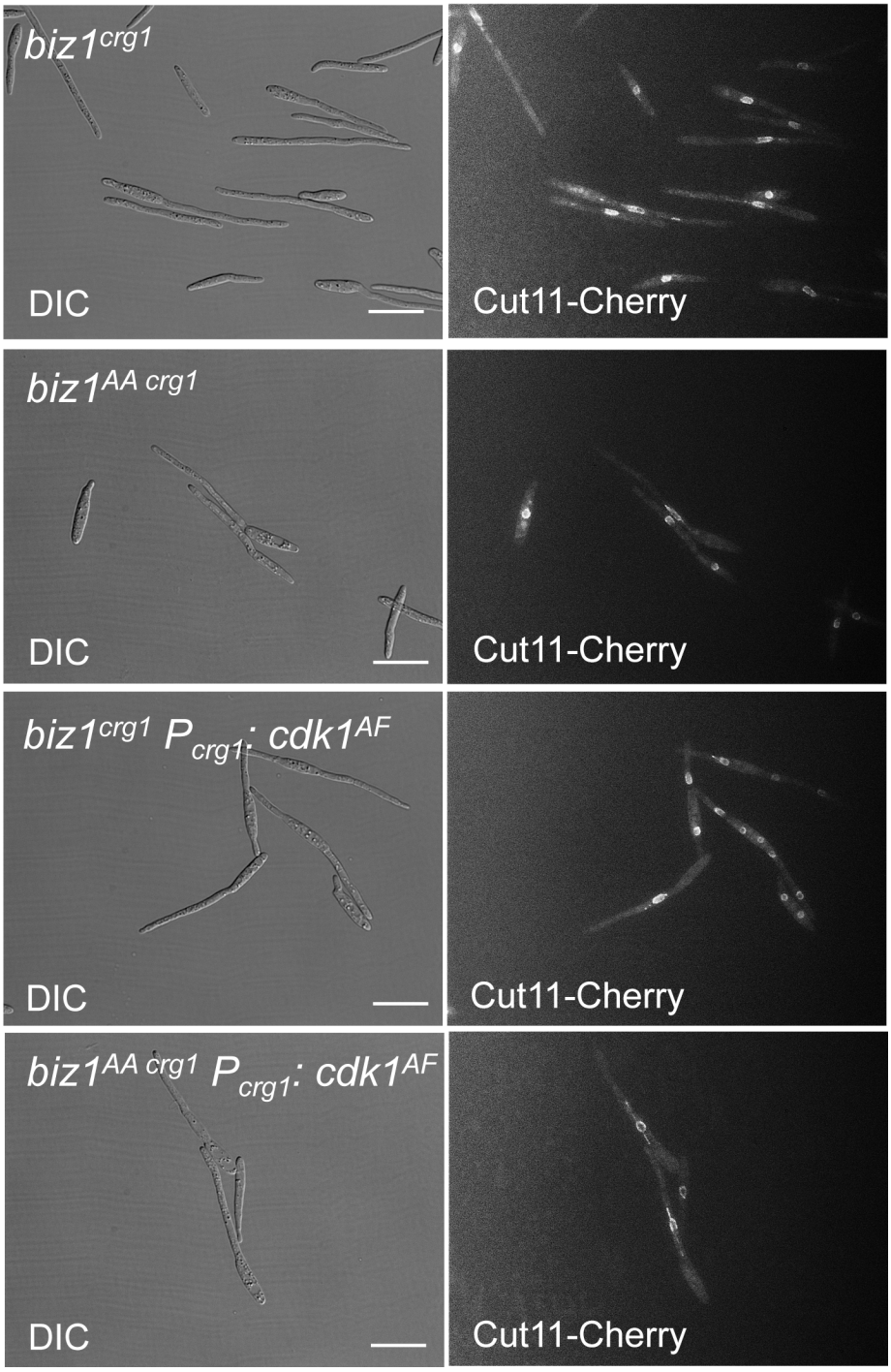

Fig. S9. The putative CDK-mediated phosphorylation of Biz1 inhibits its ability to arrest the cell cycle.

Micrographs showing cells carrying the *biz1* or *biz1^{AA}* alleles in which the endogenous promoter was exchanged by the *crg1* promoter (induced by

arabinose). Some strains also carried an ectopic copy of a transgene expressing the *cdk1*^{AF} allele under the control of *crg1* promoter. Cells were incubated for 6 hours in CMA (Complete medium plus arabinose). A fusion of a nuclear envelope protein (Cut11) to cherry was used to detect the nucleus in each cell and classify the cells in function of nuclear number (i. e. arrested or not). Ectopic expression of Biz1 induces hyperpolarized growth (10). Scale bar, 20 μm.

FIGURE S10

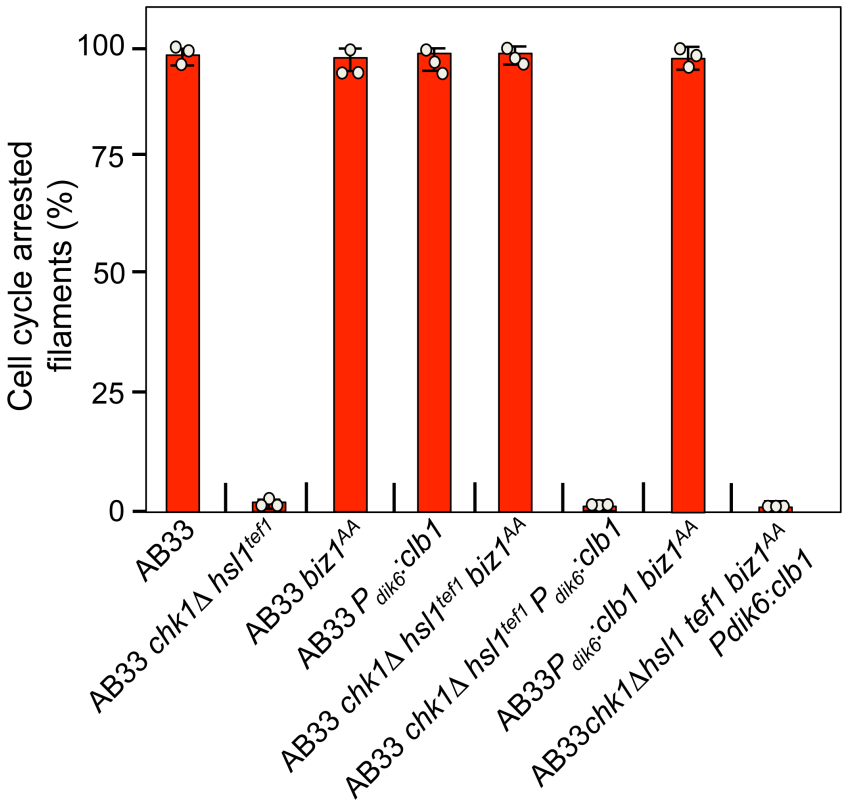

Fig. S10. Disconnecting Biz1 from cell cycle arrest during induction of the infective filament.

Graph showing the quantification of the nuclear content of AB33-derived filaments. The indicated AB33-based strains were incubated for 8 hours in minimal medium amended with nitrate to induce the genes encoding the b-factor (which are under the control of the *nar1* promoter (14)). These strains also carried an NLS-GFP transgene as a nuclear marker to address the nuclear number of each filament. Filaments carrying a single nucleus were considered as arrested on cell cycle (15). Data are presented as mean ± SD from three independent experimental replicates counting more than 50 filaments each.

FIGURE S11

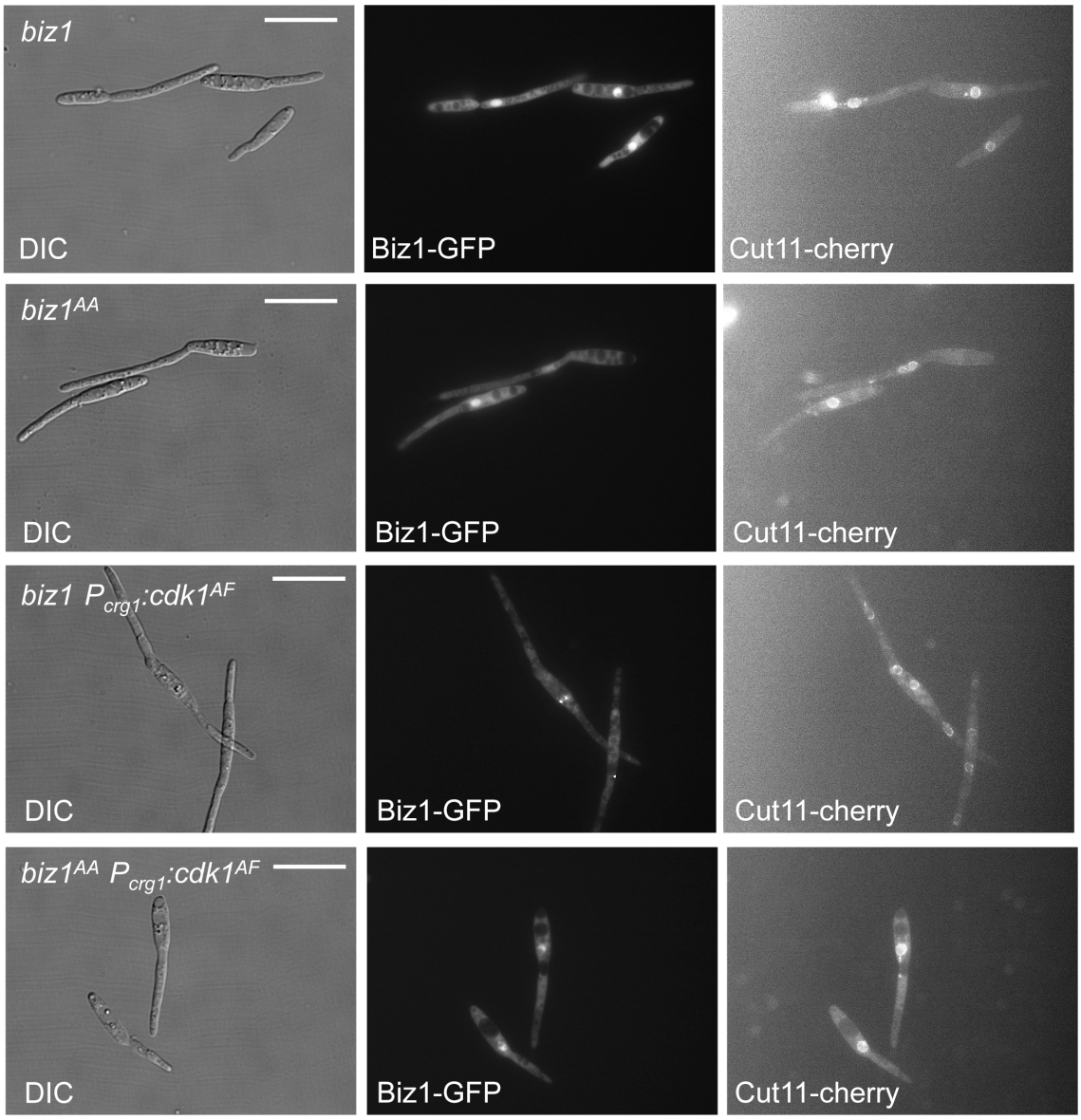

Fig. S11. CDK-mediated phosphorylation retains Biz1 at the cytoplasm. Micrographs of the indicated strains expressing or not an ectopic copy of *cdk1*^{AF} allele as well as Biz1-GFP or Biz1^{AA}-GFP fusion. The cells also carried a Cut11-cherry fusion to detect nuclear membrane. Cultures were incubated for 6 hours in inducing conditions (CMA). Scale bar, 20 μm.

FIGURE S12

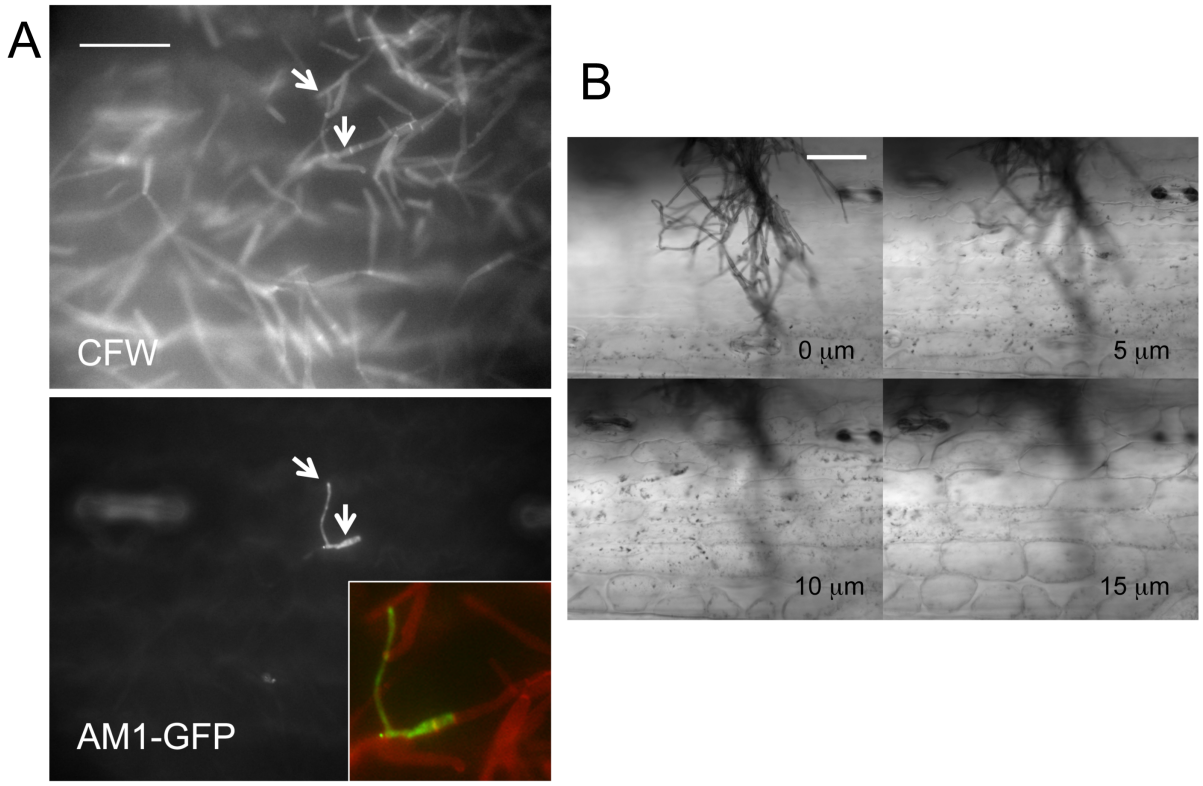

Fig. S12. Analysis of the ability of the *hsl1^{tef1} chk1Δ biz1^{AA}P$_{dik6}$:clb1* mutant strain to form appressoria formation on planta and to invade the plant tissue.

(A) We infected plants with solopathogenic cells carrying the four mutant alleles (*hsl1^{tef1} chk1Δ biz1^{AA}P$_{dik6}$*) as well as the AM1-GFP reporter. After 1 dpi, fungal material on the leaf surface was stained with calcofluor white (CFW) and expression of AM1 (GFP fluorescence) was scored with respect to specific cherry fluorescence. From 8 leaves obtained in independent infections, we were able to detect in total 6 filaments showing fluorescence. Panel A showed one representative micrograph indicating the presence of filaments expressing AM1-GFP on plant surface. This filament seemed composed by several cell compartments (separated by septa stained with CFW), and the 2-3 more apical

compartments showed GFP fluorescence (inset). Arrows pointed the tip of the filament and one of the septa. Bar: 50 μm.

(B) Series of z axis projections showing the presence of *hsl1*^{tef1} *chk1*Δ *biz1*^{AA}*P*$_{dik6}$ cells on plant surface that were unable to invade the plant tissue. Corn leave areas near the syringe puncture were collected at day 5 after infection and fungal material was visualized by staining with Chlorazole Black (11). We have analyzed 10 independent leaves, finding no evidence of plant penetration. Bar: 25 μm.

Table S1. *U. maydis* strains used in this study

Strain	Relevant genotype	Source
FB1	*a1, b1*	(16)
FB2	*a2, b2*	(16)
UMS123	*a1, b1, chk1*Δ (Hyg^R), *hsl1^{tef1}* (Nat^R)	(15)
UMS125	*a2, b2, chk1*Δ (Hyg^R), *hsl1^{tef1}* (Nat^R)	(15)
UMP368	*a1, b1, hdp2^{T607A}:frt*	This work
UMP369	*a2, b2, hdp2^{T607A}:frt*	This work
UMP370	*a1, b1, chk1*Δ (Hyg^R), *hsl1^{tef1}* (Nat^R), *hdp2^{T607A}:frt*	This work
UMP371	*a2, b2, chk1*Δ (Hyg^R), *hsl1^{tef1}* (Nat^R), *hdp2^{T607A}:frt*	This work
UMP364	*a1, b1, biz1$^{S663A\ T691A}$:frt*	This work
UMP367	*a2, b2, biz1$^{S663A\ T691A}$:frt*	This work
UMP365	*a1, b1, chk1*Δ (Hyg^R), *hsl1^{tef1}* (Nat^R), *biz1$^{S663A\ T691A}$:frt*	This work
UMP366	*a2, b2, chk1*Δ (Hyg^R), *hsl1^{tef1}* (Nat^R), *biz1$^{S663A\ T691A}$:frt*	This work
SG200	*a1, mfa2, bW2, bE1* (Phleo^R)	(6)
SG200AM1	*a1, mfa2, bW2, bE1* (Phleo^R), *ip*[*P$_{um01779}$GFPx3* (Cbx^R)]	(4)
UMP361	*a1, mfa2, bW2, bE1* (Phleo^R), *ip*[*P$_{um01779}$GFPx3* (Cbx^R)], *biz1$^{S663A\ T691A}$:frt*	This work
UMS154	*a1, mfa2, bW2, bE1* (Phleo^R), *ip*[*P$_{um01779}$GFPx3* (Cbx^R)], *chk1*Δ (Hyg^R), *hsl1^{tef1}* (Nat^R)	(15)
UMP363	*a1, mfa2, bW2, bE1* (Phleo^R), *ip*[*P$_{um01779}$GFPx3* (Cbx^R)], *chk1*Δ (Hyg^R), *hsl1^{tef1}* (Nat^R), *biz1$^{S663A\ T691A}$:frt*	This work
UMP560	*a1, mfa2, bW2, bE1* (Phleo^R), *ip*[*P$_{um01779}$GFPx3* (Cbx^R)], *chk1*Δ (Hyg^R), *hsl1^{tef1}* (Nat^R), *biz1$^{S663A\ T691A}$:frt, cut11-Cherry* (G418^R)	This work
UMC10	*a1, b1 ip*[*P$_{crg1}$:cdk1^{AF}* (Cbx^R)]	(17)
UMP382	*a1, b1, biz1^{crg1}-3HA* (G418^R, Hyg^R)	This work
UMP390	*a1, b1, biz1^{crg1}-3HA* (G418^R, Hyg^R), *ip*[*P$_{crg1}$:cdk1^{AF}* (Cbx^R)]	This work
UMP386	*a1, b1, biz1$^{crg1,\ S663A\ T691A}$-3HA* (G418^R, Hyg^R)	This work
UMP400	*a1, b1, biz1$^{crg1,\ S663A\ T691A}$-3HA* (G418^R, Hyg^R), *ip*[*P$_{crg1}$:cdk1^{AF}* (Cbx^R)]	This work
AUM331	*a1, b1, biz1^{crg1}* (G418^R), *cut11-Cherry* (Phleo^R)	This work
AUM333	*a1, b1, biz1^{crg1}* (G418^R), *cut11-Cherry* (Phleo^R), *ip*[*P$_{crg1}$:cdk1^{AF}* (Cbx^R)]	This work
AUM332	*a1, b1 biz1$^{crg1,\ S663A\ T691A}$:frt* (G418^R), *cut11-Cherry* (Phleo^R)	This work
AUM335	*a1, b1 biz1$^{crg1,\ S663A\ T691A}$:frt* (G418^R), *cut11-Cherry* (Phleo^R),	This work

	ip[P_{crg1}*:cdk1*^{AF} (Cbx^R)]	
AB33	*a2 bW2*^{nar1} *bE2*^{nar1}(Phleo^R)	(14)
UMP112	*a2, bW2*^{nar1},*bE1*^{nar1}(PhleoR), P_{dik6}*:NLS-GFP* (Cbx^R)	(15)
UMS120	*a2, bW2*^{nar1}, *bE1*^{nar1}(PhleoR), P_{dik6}*:NLS-GFP* (Cbx^R), *chk1*Δ (Hyg^R), *hsl1*^{tef1} (Nat^R)	(15)
UMP431	*a2, bW2*^{nar1}, *bE1*^{nar1}, P_{dik6}*:NLS-GFP* (Cbx^R), *biz1*$^{S663A\ T691A}$*:frt*	This work
UMP432	*a2, bW2*^{nar1}, *bE2*^{nar1}(PhleoR), P_{dik6}*:NLS-GFP* (Cbx^R), *IG*[P_{dik6}*:clb1* (G418^R)]	This work
UMP433	*a2, bW2*^{nar1}, *bE2*^{nar1}(PhleoR), *chk1*Δ (Hyg^R), *hsl1*^{tef1} (Nat^R), *biz1*$^{S663A\ T691A}$*:frt*	This work
UMP434	*a2, bW2*^{nar1}, *bE2*^{nar1}(PhleoR), *chk1*Δ (Hyg^R), *hsl1*^{tef1} (Nat^R), *IG*[P_{dik6}*:clb1* (G418^R)]	This work
UMP436	*a2, bW2*^{nar1},*bE2*^{nar1}(PhleoR), *biz1*$^{S663A\ T691A}$*:frt, IG*[P_{dik6}*:clb1* (G418^R)]	This work
UMP437	*a2, bW2*^{nar1},*bE2*^{nar1}(PhleoR), *chk1*Δ (Hyg^R), *hsl1*^{tef1} (Nat^R), *biz1*$^{S663A\ T691A}$*:frt, IG*[P_{dik6}*:clb1* (G418^R)]	This work
UMP383	*a1, b1, biz1*^{crg1}*-3HA* (G418^R, Hyg^R), *ip*[P_{crg1}*:clb1-VSV* (Cbx^R)]	This work
UMP384	*a1, b, biz1*^{crg1}*-3HA* (G418^R, Hyg^R), *ip*[P_{crg1}*:clb2-VSV* (Cbx^R)]	This work
UMP386	*a1, b1, biz1*$^{crg1,\ S663A\ T691A}$*-3HA* (G418^R, Hyg^R)	This work
UMP400	*a1, b, biz1*$^{crg1,\ S663A\ T691A}$*-3HA* (G418^R, Hyg^R), *ip*[P_{crg1}*:cdk1*^{AF} (Cbx^R)]	This work
UMP397	*a1, b1, biz1*$^{crg1,\ S663A\ T691A}$*-3HA* (G418^R, Hyg^R), *ip*[P_{crg1}*:clb2-VSV* (Cbx^R)]	This work
UMP392	*a1, b1, biz1*^{crg1}*-3HA* (G418^R, Hyg^R), *clb2*^{nar1}(Nat^R)	This work
UMP393	*a1, b1, biz1*$^{crg1,\ S663A\ T691A}$*-3HA* (G418^R, Hyg^R), *clb2*^{nar1}(Nat^R)	This work
UMP154	*a1, b1, cut11-Cherry* (Phleo^R)	(18)
AUM334	*a1, b1, cut11-Cherry* (Phleo^R), *ip*[P_{crg1}*:cdk1*^{AF} (Cbx^R)]	This work
AUM346	*a1, b1, biz1*^{crg1}*-GFP* (G418^R, Hyg^R), *cut11-Cherry* (Phleo^R)	This work
AUM349	*a1, b,1 biz1*^{crg1}*-GFP* (G418^R, Hyg^R), *cut11-Cherry* (Phleo^R), *ip*[P_{crg1}*:cdk1*^{AF} (Cbx^R)]	This work
AUM347	*a1, b1, biz1*$^{crg1,\ S663A\ T691A}$*-GFP* (G418^R, Hyg^R), *cut11-Cherry* (Phleo^R)	This work
AUM348	*a1, b,1 biz1*$^{crg1,\ S663A\ T691A}$*-GFP*(G418^R, Hyg^R), *cut11-Cherry* (Phleo^R), *ip*[P_{crg1}*:cdk1*^{AF} (Cbx^R)]	This work
UMP568	*a1, b1, biz1*^{crg1}*-GFP* (G418^R, Hyg^R), *cut11-Cherry* (Phleo^R), *ip*[P_{crg1}*:cdk1*^{AF} (Cbx^R)], *bmh1*^{nar1} *(Nat^R)*	This work
UMP406	*a1, b1, biz1*^{crg1}*-GFP* (G418^R, Hyg^R), *bmh1-3HA*(Nat^R)	This work
UMP407	*a1, b1, biz1*^{crg1}*-GFP* (G418^R, Hyg^R), *bmh1-3HA*(Nat^R), *ip*[P_{crg1}*:cdk1*^{AF} (Cbx^R)]	This work

UMP408	*a1, b1, biz1$^{crg1,\ S663A\ T691A}$-GFP* (G418^{R}, Hyg^{R}), *bmh1-3HA*(Nat^{R})	This work
UMP409	*a1, b1, biz1$^{crg1,\ S663A\ T691A}$-GFP*(G418^{R}, Hyg^{R}), *bmh1-3HA*(Nat^{R}), *ip*[P_{crg1}*:cdk1^{AF}* (Cbx^{R})]	This work
UMP520	*a1, mfa2, bW2, bE1* (Phleo^{R}), *ip*[$P_{um01779}$*GFPx3* (Cbx^{R})], *chk1*Δ (Hyg^{R}), *hsl1^{tef1}* (Nat^{R}), *biz1$^{S663A\ T691A}$:frt, IG*[P_{dik6}*:clb1* (G418^{R})]	This work
UMS131	*a1, mfa2, bW2, bE1* (Phleo^{R}), *chk1*Δ (Hyg^{R}), *hsl1^{tef1}* (Nat^{R})	(15)
UMP360	*a1, mfa2, bW2, bE1* (Phleo^{R}), *biz1$^{S663A\ T691A}$:frt*	This work
UMN69	*a1, mfa2, bW2, bE1* (Phleo^{R}), *ip*[P_{dik6}*:clb1* (Cbx^{R})],	(10)
UMP500	*a1, mfa2, bW2, bE1* (Phleo^{R}), *chk1*Δ (Hyg^{R}), *hsl1^{tef1}* (Nat^{R}), *biz1$^{S663A\ T691A}$:frt*	This work
UMP501	*a1, mfa2, bW2, bE1* (Phleo^{R}), *chk1*Δ (Hyg^{R}), *hsl1^{tef1}* (Nat^{R}), *ip*[P_{dik6}*:clb1* (Cbx^{R})],	This work
UMP502	*a1, mfa2, bW2, bE1* (Phleo^{R}), *ip*[P_{dik6}*:clb1* (Cbx^{R})], *biz1$^{S663A\ T691A}$:frt*	This work
UMP503	*a1, mfa2, bW2, bE1* (Phleo^{R}), *chk1*Δ (Hyg^{R}), *hsl1^{tef1}* (Nat^{R}), *biz1$^{S663A\ T691A}$:frt, ip*[P_{dik6}*:clb1* (Cbx^{R})].	This work
UMS155	*a1, mfa2, bW2, bE1* (Phleo^{R}), *ip*[$P_{um01779}$*GFPx3* (Cbx^{R})], *IG*[P_{crg1}*:fuz7^{DD}* (G418^{R})]	(15)
UMS156	*a1, mfa2, bW2, bE1* (Phleo^{R}), *ip*[$P_{um01779}$*GFPx3* (Cbx^{R})], *chk1*Δ (Hyg^{R}), *hsl1^{tef1}* (Nat^{R}), *IG*[P_{crg1}*:fuz7^{DD}* (G418^{R})]	(15)
UMS186	*a1, mfa2, bW2, bE1* (Phleo^{R}), *ip*[$P_{um01779}$*GFPx3* (Cbx^{R})], *IG*[P_{crg1}*:kpp6$^{P130A\ P131A}$* (G418^{R})]	This work
UMS187	*a1, mfa2, bW2, bE1* (Phleo^{R}), *ip*[$P_{um01779}$*GFPx3* (Cbx^{R})], *chk1*Δ (Hyg^{R}), *hsl1^{tef1}* (Nat^{R}), *IG*[P_{crg1}*:kpp6$^{P130A\ P131A}$* (G418^{R})]	This work
UMP565	*a1, mfa2, bW2, bE1* (Phleo^{R}), *chk1*Δ (Hyg^{R}), *hsl1^{tef1}* (Nat^{R}), *biz1^{S663A}:frt*	This work
UMP566	*a1, mfa2, bW2, bE1* (Phleo^{R}), *chk1*Δ (Hyg^{R}), *hsl1^{tef1}* (Nat^{R}), *biz ^{T691A}:frt*	This work
UMP567	*a1, mfa2, bW2, bE1* (Phleo^{R}), *chk1*Δ (Hyg^{R}), *hsl1^{tef1}* (Nat^{R}), *biz1$^{S663D\ T691D}$:frt*	This work
UMS191	*a1, mfa2, bW2, bE1* (Phleo^{R}), *ip*[$P_{um01779}$*GFPx3* (Cbx^{R})], *chk1*Δ (Hyg^{R}), *hsl1^{tef1}* (Nat^{R}), *IG*[P_{tef1}*:Cherry* (G418^{R})]	(15)
UMP571	*a1, mfa2, bW2, bE1* (Phleo^{R}), *ip*[$P_{um01779}$*GFPx3* (Cbx^{R})], *chk1*Δ (Hyg^{R}), *hsl1^{tef1}* (Nat^{R}), *biz1$^{S663A\ T691A}$:frt, IG*[P_{tef1}*:Cherry* (G418^{R})]	This work

Table S2. Oligonucleotides used in this study

HDP2-1	5'ctaggtctcgcctgcgtttaAACCCGTCAATTGCGGAGCGTGCCGAG3'
HDP2-2	5'CGGGCTCGGCGCCCATTCGCATCGGAGcGCGGAAGTTGTGCCATGCCGCCGAACC3'
HDP2-3	5'GGTTCGGCGGCATGGCACAACTTCCGCgCTCCGATGCGAATGGGCGCCGAGCCCG3'
HDP2-4	5'ctaggtctccaggccTTAGGGTTCAGCAGCGGCAGCGT3'
HDP2-5	5'tagggtctccggccGACTCGGCTTACATCGCACGACTCGGG3'
HDP2-6	5'ctaggtctcgctgcgtttaAACGATATCTGGCTCACCTCTTCCCAA3'
BIZ1-1	5'tagggtctccggccAGCATGGGCGAAAGCTGACTCGACTGC3'
BIZ1-2	5'ctaggtctcgctgcgtttaAACCTCAACTGACTTACCAACGGTGAG3'
BIZ1CRG-1	5'ctaggtctcgcctgcgtttaAACCTGTCGTGATCCCGAAGATCCCGT3'
BIZ1CRG-2	5'ctaggtctccaggccGCTGTTTCAAGCACACTGGCCCTCGAG3'
BIZ1CRG-3	5'ctaggtctccggccATGTCGATGCTTAGCACACGGGCAACT3'
BIZ1CRG-4	5'ctaggtctcgctgcgtttaAACTTATGCGACTGTGGTAGTCGGCCA3'
Biz1GFP-1	5'ctaggtctcgcctgcgtttAAACTGGCACGGCGGCAGCTACGGAAT3'
Biz1GFP-2	5'ctaggtctcttggccCAACGACGGCTGGTGTGACCACCTTGC3'
Biz1GFP-3	5'ctaggtctccggccAGCATGGGCGAAAGCTGACTCGACTGC3'
Biz1GFP-4	5'ctaggtctcgctgcgtttaAACCTCAACTGACTTACCAACGGTGAG3'

Table S3. Raw data for infection assays from Figure 1B

Replicate 1								
Cross	No Symptoms	Chlorosis	Ligula Swelling	Small tumors <2 mm	Large tumors >2 mm	Tumors causing stem bending	Dead plants	Total infected plants
control	0	0	0	2	15	10	3	30
*chk1*Δ *hsl1*^{tef1}	8	21	1	0	0	0	0	30
hdp2^{T607A}				5	11	10	4	30
*chk1*Δ *hsl1*^{tef1} *hdp2*^{T607A}	8	20	0	0	0	0	0	28
biz1$^{S663A, T691A}$	0	0	3	4	11	11	1	30
*chk1*Δ *hsl1*^{tef1} *biz1*$^{S663A, T691A}$	2	3	3	21	0	0	0	29
water	17	8	0	0	0	0	0	25

Replicate 2								
Cross	No Symptoms	Chlorosis	Ligula Swelling	Small tumors <2 mm	Large tumors >2 mm	Tumors causing stem bending	Dead plants	Total infected plants
control	0	0	0	4	13	8	4	29
*chk1*Δ *hsl1*^{tef1}	11	18	0	1	0	0	0	30
hdp2^{T607A}	0	0	0	7	10	10	3	30
*chk1*Δ *hsl1*^{tef1} *hdp2*^{T607A}	14	16	0	0	0	0	0	30
biz1$^{S663A, T691A}$	0	0	0	4	9	9	4	26
*chk1*Δ *hsl1*^{tef1} *biz1*$^{S663A, T691A}$	2	5	1	22	0	0	0	30
water	20	9	0	0	0	0	0	29

Replicate 3

Cross	No Symptoms	Chlorosis	Ligula Swelling	Small tumors <2 mm	Large tumors >2 mm	Tumors causing stem bending	Dead plants	Total infected plants
control	0	0	2	3	16	9	0	30
*chk1*Δ *hsl1*^{tef1}	24	6	0	0	0	0	0	30
hdp2^{T607A}	0	0	3	4	12	7	1	27
*chk1*Δ *hsl1*^{tef1} *hdp2*^{T607A}	19	11	0	0	0	0	0	30
biz1$^{S663A, T691A}$	0	0	0	7	18	4	0	29
*chk1*Δ *hsl1*^{tef1} *biz1*$^{S663A, T691A}$	0	3	3	24	0	0	0	30
water	23	7	0	0	0	0	0	30

Table S4. Raw data for infection assays from Figure S2

Replicate 1								
SG200 derived strain	No Symptoms	Chlorosis	Ligula Swelling	Small tumors <2 mm	Large tumors >2 mm	Tumors causing stem bending	Dead plants	Total infected plants
control	0	2	1	16	8	3	0	30
*chk1*Δ *hsl1*^{tef1}	20	10	0	0	0	0	0	30
*chk1*Δ *hsl1*^{tef1} *biz1*$^{S663A, T691A}$	4	7	0	18	0	0	0	29
*chk1*Δ *hsl1*^{tef1} *biz1*^{S663A}	22	8	0	0	0	0	0	30
*chk1*Δ *hsl1*^{tef1} *biz* ^{T691A}	24	6	0	0	0	0	0	30
*chk1*Δ *hsl1*^{tef1} *biz1*$^{S663D, T691D}$	3	6	0	21	0	0	0	30
water	25	2	0	0	0	0	0	27

Replicate 2								
SG200 derived strain	No Symptoms	Chlorosis	Ligula Swelling	Small tumors <2 mm	Large tumors >2 mm	Tumors causing stem bending	Dead plants	Total infected plants
control	1	4	0	14	7	3	0	29
*chk1*Δ *hsl1*^{tef1}	18	12	0	0	0	0	0	30
*chk1*Δ *hsl1*^{tef1} *biz1*$^{S663A, T691A}$	6	8	1	15	0	0	0	30
*chk1*Δ *hsl1*^{tef1} *biz1*^{S663A}	19	11	0	0	0	0	0	30
*chk1*Δ *hsl1*^{tef1} *biz* ^{T691A}	23	7	0	0	0	0	0	30
*chk1*Δ *hsl1*^{tef1}	2	8	2	18	0	0	0	30

biz1$^{S663D, T691D}$								
water	23	7	0	0	0	0	0	30

Replicate 3								
SG200 derived strain	No Symptoms	Chlorosis	Ligula Swelling	Small tumors <2 mm	Large tumors >2 mm	Tumors causing stem bending	Dead plants	Total infected plants
control	0	3	3	14	5	5	0	30
*chk1*Δ *hsl1*^{tef1}	16	14	0	0	0	0	0	30
*chk1*Δ *hsl1*^{tef1} *biz1*$^{S663A, T691A}$	2	3	2	23	0	0	0	30
*chk1*Δ *hsl1*^{tef1} *biz1*^{S663A}	19	11	0	0	0	0	0	30
*chk1*Δ *hsl1*^{tef1} *biz* ^{T691A}	24	6	0	0	0	0	0	30
*chk1*Δ *hsl1*^{tef1} *biz1*$^{S663D, T691D}$	0	5	2	23	0	0	0	30
water	21	9	0	0	0	0	0	30

Table S5. Raw data for infection assays from Figure 5D

Replicate 1								
SG200 derived strain	No Symptoms	Chlorosis	Ligula Swelling	Small tumors <2 mm	Large tumors >2 mm	Tumors causing stem bending	Dead plants	Total infected plants
control	0	3	0	16	8	3	0	30
*chk1*Δ *hsl1*^{tef1}	20	10	0	0	0	0	0	30
biz1^{AA}	0	1	0	16	9	4	0	30
P_{dik6}:*clb1*	1	10	2	12	4	0	0	29
*chk1*Δ *hsl1*^{tef1} *biz* ^{AA}	3	8	1	18	0	0	0	30
*chk1*Δ *hsl1*^{tef1} P_{dik6}:*clb1*	26	4	0	0	0	0	0	30
P_{dik6}:*clb1* *biz1*^{AA}	4	9	0	15	2	0	0	30
*chk1*Δ *hsl1*^{tef1} P_{dik6}:*clb1* *biz* ^{AA}	18	12	0	0	0	0	0	30

Replicate 2								
SG200 derived strain	No Symptoms	Chlorosis	Ligula Swelling	Small tumors <2 mm	Large tumors >2 mm	Tumors causing stem bending	Dead plants	Total infected plants
control	1	2	1	17	6	3	0	30
*chk1*Δ *hsl1*^{tef1}	18	12	0	0	0	0	0	30
biz1^{AA}	2	2	1	18	5	2	0	30
P_{dik6}:*clb1*	3	10	1	16	0	0	0	30
*chk1*Δ *hsl1*^{tef1} *biz* ^{AA}	5	5	1	19	0	0	0	30
*chk1*Δ *hsl1*^{tef1} P_{dik6}:*clb1*	25	5	0	0	0	0	0	30
P_{dik6}:*clb1* *biz1*^{AA}	6	5	2	13	3	0	0	29
*chk1*Δ *hsl1*^{tef1} P_{dik6}:*clb1* *biz* ^{AA}	24	6	0	0	0	0	0	30

Replicate 3								
SG200 derived strain	No Symptoms	Chlorosis	Ligula Swelling	Small tumors <2 mm	Large tumors >2 mm	Tumors causing stem bending	Dead plants	Total infected plants
control	0	1	2	18	9	0	0	30
chk1Δ hsl1^{tef1}	21	9	0	0	0	0	0	30
biz1^{AA}	0	0	2	21	5	2	0	30
P$_{dik6:}$clb1	4	2	1	15	0	0	0	30
chk1Δ hsl1^{tef1} biz^{AA}	2	6	0	22	0	0	0	30
chk1Δ hsl1^{tef1} P$_{dik6:}$clb1	23	7	0	0	0	0	0	30
P$_{dik6:}$clb1 biz1^{AA}	3	4	2	14	7	0	0	30
chk1Δ hsl1^{tef1} P$_{dik6:}$clb1 biz^{AA}	27	3	0	0	0	0	0	30

SI References

1. Y. Khrunyk, K. Munch, K. Schipper, A. N. Lupas, R. Kahmann, The use of FLP-mediated recombination for the functional analysis of an effector gene family in the biotrophic smut fungus Ustilago maydis. *New Phytol.* **187**, 957-968 (2010).
2. M. Terfruchte *et al.*, Establishing a versatile Golden Gate cloning system for genetic engineering in fungi. *Fung. Genet. Biol.* **62**, 1-10 (2014).
3. D. Lanver, A. Mendoza-Mendoza, A. Brachmann, R. Kahmann, Sho1 and Msb2-related proteins regulate appressorium development in the smut fungus Ustilago maydis. *Plant Cell* **22**, 2085-2101 (2010).
4. A. Mendoza-Mendoza *et al.*, Physical-chemical plant-derived signals induce differentiation in Ustilago maydis. *Mol. Microb.* **71**, 895-911 (2009).
5. D. Lanver *et al.*, Plant surface cues prime Ustilago maydis for biotrophic development. *PLoS Pathog* **10**, e1004272 (2014).
6. M. Bolker, S. Genin, C. Lehmler, R. Kahmann, Genetic regulation of mating and dimorphism in Ustilago maydis. *Can. J. Bot.* **73**, S320-S325 (1995).
7. P. Muller, G. Weinzierl, A. Brachmann, M. Feldbrugge, R. Kahmann, Mating and pathogenic development of the Smut fungus Ustilago maydis are regulated by one mitogen-activated protein kinase cascade. *Eukaryot. Cell* **2**, 1187-1199 (2003).
8. M. B. Yaffe *et al.*, The structural basis for 14-3-3:phosphopeptide binding specificity. *Cell* **91**, 961-971 (1997).
9. C. Johnson *et al.*, Bioinformatic and experimental survey of 14-3-3-binding sites. *Biochem. J.* **427**, 69-78 (2010).
10. I. Flor-Parra, M. Vranes, J. Kamper, J. Perez-Martin, Biz1, a zinc finger protein required for plant invasion by Ustilago maydis, regulates the levels of a mitotic cyclin. *Plant Cell* **18**, 2369-2387 (2006).
11. A. Brachmann, J. Schirawski, P. Müller, R. Kahmann, An unusual MAP kinase is required for efficient penetration of the plant surface by Ustilago maydis. *EMBO J.* **22**, 2199-2210 (2003).

12. C. de Sena-Tomas, A. Fernandez-Alvarez, W. K. Holloman, J. Perez-Martin, The DNA damage response signaling cascade regulates proliferation of the phytopathogenic fungus Ustilago maydis in planta. *Plant Cell* **23**, 1654-1665 (2011).
13. C. de Sena-Tomas, M. Navarro-Gonzalez, U. Kues, J. Perez-Martin, A DNA damage checkpoint pathway coordinates the division of dikaryotic cells in the ink cap mushroom Coprinopsis cinerea. *Genetics* **195**, 47-57 (2013).
14. A. Brachmann, G. Weinzierl, J. Kamper, R. Kahmann, Identification of genes in the bW/bE regulatory cascade in Ustilago maydis. *Mol. Microb.* **42**, 1047-1063 (2001).
15. S. Castanheira, N. Mielnichuk, J. Perez-Martin, Programmed cell cycle arrest is required for infection of corn plants by the fungus Ustilago maydis. *Development* **141**, 4817-4826 (2014).
16. F. Banuett, I. Herskowitz, Different a alleles of Ustilago maydis are necessary for maintenance of filamentous growth but not for meiosis. *Proc. Natl. Acad. Sci. U S A* **86**, 5878-5882 (1989).
17. C. Sgarlata, J. Perez-Martin, Inhibitory phosphorylation of a mitotic cyclin-dependent kinase regulates the morphogenesis, cell size and virulence of the smut fungus Ustilago maydis. *J. Cell Sci.* **118**, 3607-3622 (2005).
18. J. Perez-Martin, DNA-damage response in the basidiomycete fungus Ustilago maydis relies in a sole Chk1-like kinase. *DNA Repair* **8**, 720-731 (2009).